PROCEEDINGS OF SCIENCE

Geomagnetic Diurnal Transitions of Positron and Electron Flux at 20 – 300 MeV as Observed by the AESOP-Lite Balloon Payload

Scott Martin,[a,*] **John M. Clem,**[a] **Paul A. Evenson,**[a] **Robert P. Johnson,**[b] **Brian Lucas,**[a] **Pierre-Simon Mangeard**[a] **and James Roth**[a]

[a] *Bartol Research Institute, University of Delaware Department of Physics and Astronomy, 104 The Green, Newark DE, USA*

[b] *Santa Cruz Institute for Particle Physics, University of California Santa Cruz, 1156 High St., Santa Cruz, CA, USA*

E-mail: srmartin@udel.edu, jmc@udel.edu, evenson@udel.edu, rjohnson@ucsc.edu, lucasb@udel.edu, mangeard@udel.edu, roth@udel.edu

There are two dominant sources of low-energy electrons and positrons (20 MeV – 1 GeV) observed at the top of the atmosphere: cosmic rays, and atmospheric secondaries. The latter are produced by the interaction of Cosmic Ray nuclei in the atmosphere either directly above the detector or near the magnetic conjugate point. Upwards-moving secondaries at the conjugate point that have a rigidity lower than the local geomagnetic cutoff can become trapped along the geomagnetic field lines and re-enter the atmosphere by the detector. These are referred to as re-entrant splash albedo. These particles escape the geomagnetic field if their rigidity exceeds the local geomagnetic cutoff. At high latitude, the geomagnetic cutoff depends on location and time. The cutoff is effectively zero during nighttime when the albedo particles of any rigidity can escape via the magnetotail. Thus, the re-entrant albedo enhances the observed flux only during the daytime when the geomagnetic cutoff is non-zero. The balloon-borne spectrometer AESOP-Lite (Anti-Electron Sub-Orbital Payload Low Energy) observed these diurnal transitions at energies between 20 MeV and 300 MeV during its May 2018 flight from Kiruna, Sweden to Ellesmere Island, Canada. These observations show a time difference in the diurnal geomagnetic cutoff transitions between electrons and positrons. We simulate the trajectory of these particles observed during the 2018 flight to investigate the charge-sign and rigidity dependence of their paths through the magnetosphere during the day-night transitions.

38th International Cosmic Ray Conference (ICRC2023)
26 July - 3 August, 2023
Nagoya, Japan

*Speaker

PoS(ICRC2023)1329

1. Introduction

Charged particles in the upper atmosphere are classified according to their source. Cosmic rays are charged particles originating from the interplanetary medium that propagate through the magnetosphere and enter with the atmosphere. Atmospheric secondaries are particles produced by the interaction of cosmic ray nuclei in the atmosphere. These interactions include ionization, bremsstrahlung, and electromagnetic cascades [2, 5]. Electron and positron secondaries can travel upwards and leave the atmosphere, at which point they are considered splash albedo. If the particle's rigidity does not exceed the local geomagnetic cutoff, it will travel along the Earth's field lines and reenter the atmosphere, at which point it becomes "reentrant splash albedo", or "reentrant albedo". Reentrant albedo can escape the magnetic field if their rigidity exceeds the geomagnetic cutoff. Similarly, cosmic rays cannot penetrate a certain region of the magnetosphere if their rigidity does not exceed the local cutoff. As a result, the observed electron and positron flux spectra will change as the cutoff varies. We expect a decrease in cosmic ray flux in the atmosphere at energies lower than the cutoff, as they lack the momentum to penetrate into the atmosphere. Conversely, we expect a higher flux for reentrant albedo at energies below the cutoff, as these particles lack the momentum to escape the magnetosphere and remain trapped in the atmosphere. At energies higher than the cutoff cosmic ray electron flux will dominate over reentrant albedo, as cosmic rays will penetrate the atmosphere while reentrant albedo will escape the magnetic field [1].

Geomagnetic cutoff varies with latitude, time, and the structure of the magnetosphere. On the daytime side of the planet the solar wind is flowing into the planet, interacting with the Earth's magnetic field to create a barrier that requires a higher rigidity to penetrate. As a result, reentrant albedo will dominate the low energy electron and positron flux spectra over cosmic rays. Conversely, on the nighttime side of the planet the solar wind flows away from the Earth, stretching the magnetic field lines to the magnetotail. Here the cutoff is effectively zero, so reentrant albedo electrons of all rigidities will be able to escape the magnetosphere. Cosmic ray electrons of all rigidities will be able to penetrate the atmosphere for the same reason. Therefore, cosmic ray electrons will dominate the low energy flux spectrum over the reentrant albedo when observed from within the atmosphere on the night side of the planet. During a transition from night to day, one can observe the transition in the electron and positron flux spectra as the dominant source of particles changes.

2. AESOP-Lite 2018 Campaign

In May 2018, the balloon-borne spectrometer AESOP-Lite (Anti-Electron Sub-Orbital Payload Low Energy) launched from Kiruna, Sweden with the primary science objective of measuring the low-energy spectra (20MeV - 1GeV) of cosmic ray electrons and positrons [4]. The flight lasted for over 130 hours, floating at an average altitude of 3 gcm^{-2} before landing in Ellesmere Island, Canada. With seven silicon strip detectors and a dipole magnet, the instrument is able to track a particle and determine the particle type and rigidity. A gas Cherenkov detector is also employed in particle type determination. By floating in the northern polar region of the Earth, AESOP-Lite was able to observe the diurnal variation in electron and positron flux mentioned above. The AESOP-Lite group computed the geomagnetic cutoff for electrons and positrons for the duration of the flight using a code [3] that takes into account the International Geomagnetic Reference Field (IGRF) and

the Tsyganenko model of the magnetosphere [6]. These results were then compared to apparent transitions in the flight data to determine the time of the diurnal transitions. As [4] explains, there were limitations to their ability to determine the geomagnetic cutoff. The Kp index is defined in three hour intervals, causing sudden jumps in the cutoff time series. Between hours 17 and 32 of the flight, the cutoff simulation and flight data did not agree, so they were unable to determine if the instrument was in daytime or nighttime. The goal of this project is to employ a third method of determining the cutoff and to compare that with the methods used in the 2018 campaign.

Both analysis methods from the 2018 campaign exposed a lag in the timing between the positron and electron cutoff transition, with the positron transition leading the electron transition by 2-3 hours during some transitions. This charge sign dependence in the cutoff transition timing has not been studied at length. Another goal of this project is to quantify and understand this charge sign dependence using a more precise method of determining the cutoff.

3. Methods

We employ a novel method of determining the geomagnetic cutoff that fits observed data from the AESOP-Lite campaign to simulated flux at the instrument location. We consider the dominant sources of electrons at the detection site: galactic cosmic ray (GCR) electrons, secondary electrons created from interactions of GCR electrons and positrons, reentrant albedo (RA) electrons, and secondaries created from interactions of RA electrons and positrons. The 2018 campaign determined the electron and positron flux spectra at the top of the atmosphere (TOA) for both GCRs and RA. We employ a Monte Carlo simulation that takes a distribution of electrons and positrons determined by the TOA spectra and propagates them through the atmosphere to certain atmospheric depths ranging from 0.87537 gcm^{-2} to 3.37758 gcm^{-2} so that we can determine the flux spectra at the top of the payload (TOP) at different depths. We can manually apply a cutoff to each flux source by defining all TOA flux above a certain cutoff to be zero for GCR electrons and positrons, and all TOA flux below that cutoff to be zero for RA electrons and positrons. The TOP flux spectra then follows this equation:

$$Flux(E_{TOP}) = \begin{Bmatrix} NIS(E_{TOP}) + RAEbE(E_{TOP}) + RAPbE(E_{TOP}), & if E_{TOA} < E_{cutoff} \\ NIS(E_{TOP}) + EbE(E_{TOP}) + PbE(E_{TOP}), & if E_{TOA} > E_{cutoff} \end{Bmatrix}, \tag{1}$$

where NIS is nucleonic-induced secondaries, RAEbE and RAPbE are reentrant albedo electron-borne electrons and reentrant albedo positron-borne electrons, and EbE and PbE are GCR electron-borne electrons and GCR positron-borne electrons.

Nucleonic secondaries as determined by a calculation based on the defined atmospheric depth. We assume that nucleonic secondaries are unaffected by geomagnetic cutoff, but further analysis is needed to determine if this assumption is correct.

The 2018 AESOP-Lite campaign measured the TOP flux in 30 minute time bins. To determine the cutoff at the payload, we match the payload's atmospheric depth to the nearest simulated atmospheric depth. The uncertainty in the depth is considered large enough that the simulated depth does not need to be the same as the payload depth. We then determine the TOP spectra of the

five sources for cutoffs ranging from 0 to 500 MeV/c, which is greater than 200 MeV/c higher than the highest cutoff determined by simulations from the 2018 campaign, in steps of 10 MeV/c. These spectra are added to create a total TOP flux spectra. For each cutoff, we fit the observed spectra to the simulated spectra and employ a χ^2 goodness of fit test to determine which cutoff results in the best fit to the data. That cutoff is then considered the electron geomagnetic cutoff at that time and location. The results of this fit will then be compared to the simulated cutoff calculation from the 2018 campaign to determine the validity of this novel cutoff calculation method, as well as to study the timing of the cutoff transitions.

4. Analysis

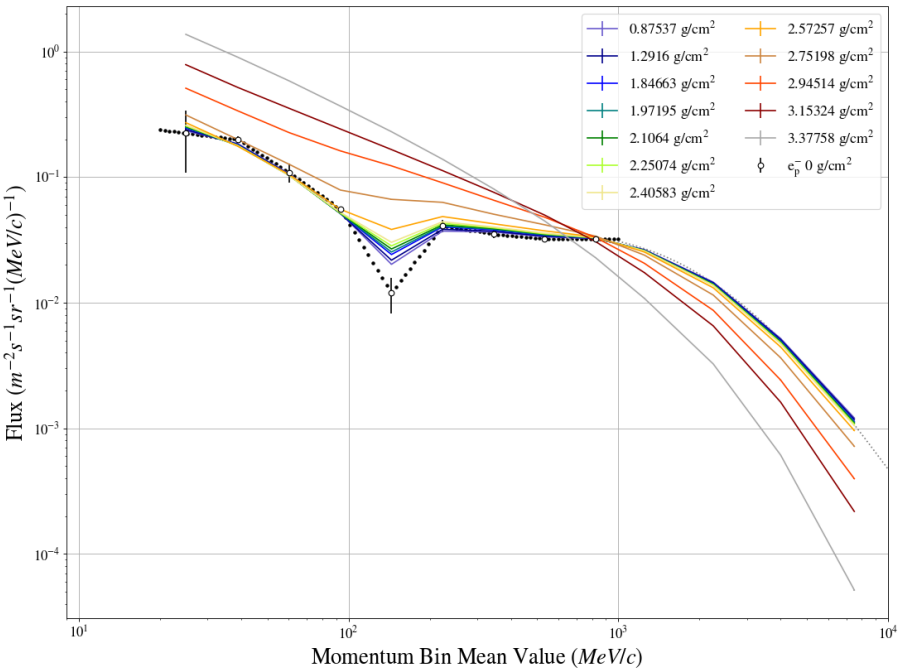

Figure 1: Simulated TOP flux spectra of electrons borne from GCR electrons at different atmospheric depths. The TOA spectrum is from the measurements made during the 2018 AESOP-Lite campaign. The TOA spectrum was propagated to different depths in a Monte-Carlo simulation.

We begin with the GCR electrons spectrum at TOA. We employ the Monte-Carlo simulation to propagate this distribution of electrons through the atmosphere to different atmospheric depths. The simulation accounts for interactions between these electrons and particles inhabiting the upper atmosphere. The TOP spectra at different depths can be found in Figure 1. At energies higher than 10^3 MeV, flux decreases as depth increases due to higher energy electrons losing energy through interaction. Flux increases at energies lower than 10^3 MeV due to spillover from the higher energy electrons. The spectra accounts for both GCR electrons and the secondaries produced from their

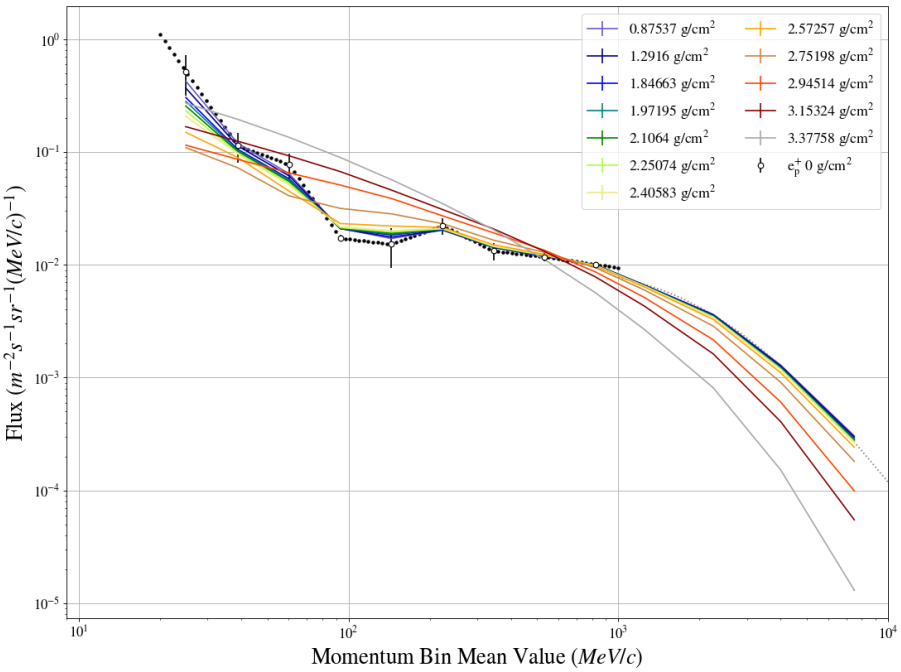

Figure 2: Simulated TOP flux spectra of positrons borne from GCR positrons at different atmospheric depths. The TOA spectrum is from the measurements made during the 2018 AESOP-Lite campaign. The TOA spectrum was propagated to different depths in a Monte-Carlo simulation.

interactions, so the increase in flux accounts for both the primaries losing energy and secondary electrons that are the product of interactions like ionization. The positron distribution at different depths follows a similar pattern, with flux decrease seen when momentum is greater than 250 MeV/c and flux increase seen at midrange energies (Figure 2). Unlike electrons, the positron spectra have another decrease in flux with an increase in depth in the lower energy range. More research is needed to determine the cause of this difference.

For the electron and positron reentrant albedo, the TOA distribution was also propagated to different atmospheric depths using the same Monte-Carlo simulation. The 2018 campaign only determined a reentrant albedo spectrum for energies ranging from 24.93 MeV to 93.23 MeV, so we used a power law fit with an index of -1.6 ± 0.1 to interpolate the spectra over the full energy range we were considering. As the atmospheric depth decreases, both electron and positron flux decrease over the entire range of energies.

At a given atmospheric depth, the contributions from reentrant albedo, GCR, and nucleonic-induced secondaries were summed to create a total estimated flux spectrum at that depth. An artificial geomagnetic cutoff is applied to the reentrant albedo and GCR source in accordance with equation 1. Figures 4 and 5 illustrate a case at an atmospheric depth of 2.1064 g/cm^2. This example ignores the nucleonic-induced electrons, as we assume the flux spectrum is unaffected by the cutoff. An arbitrary cutoff is applied to the electron distributions. At energies below the cutoff, the total

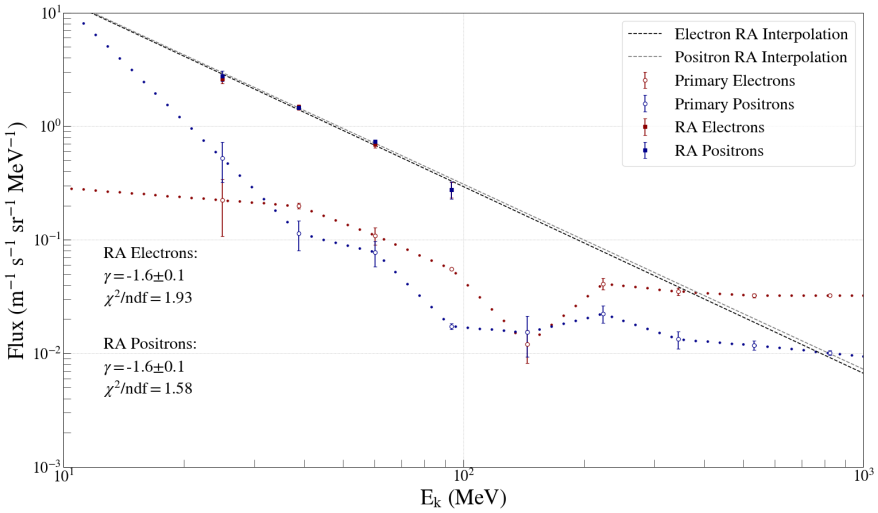

Figure 3: Power law fit of the electron and positron reentrant albedo spectra measured during the 2018 AESOP-Lite campaign.

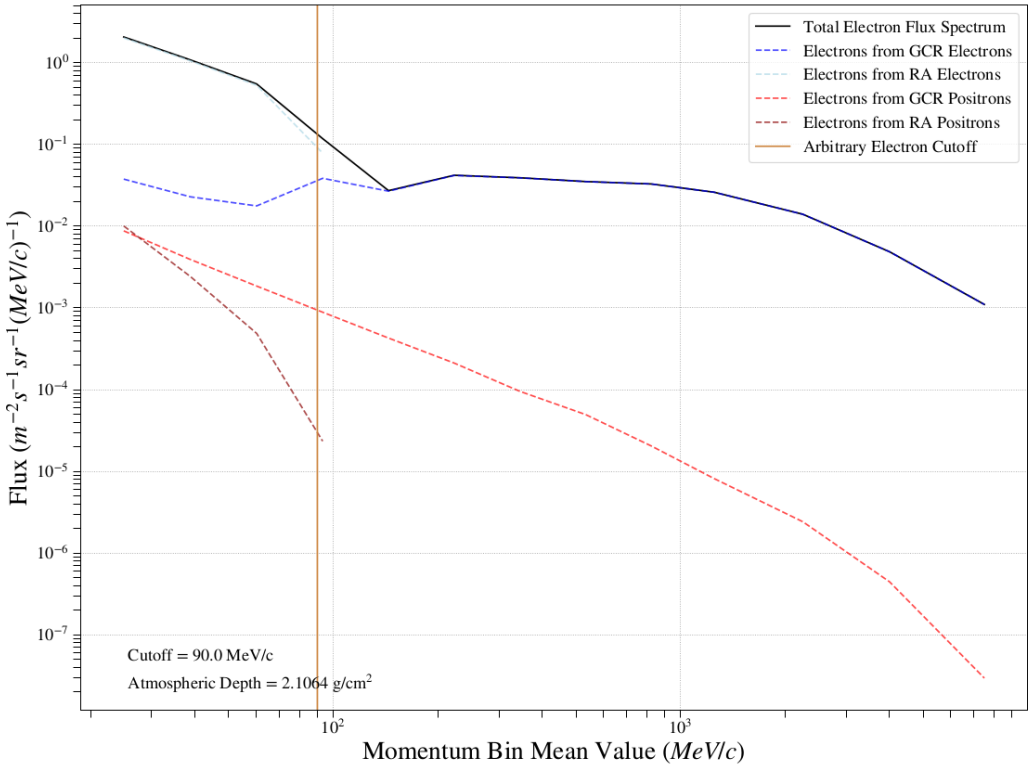

Figure 4: Estimated total flux spectrum with the spectra of the cutoff-dependent electron sources at an atmospheric depth of 2.1064 g/cm^2. An arbitrary cutoff of 90 MeV/c is applied to each source to illustrate the spectra at a lower cutoff.

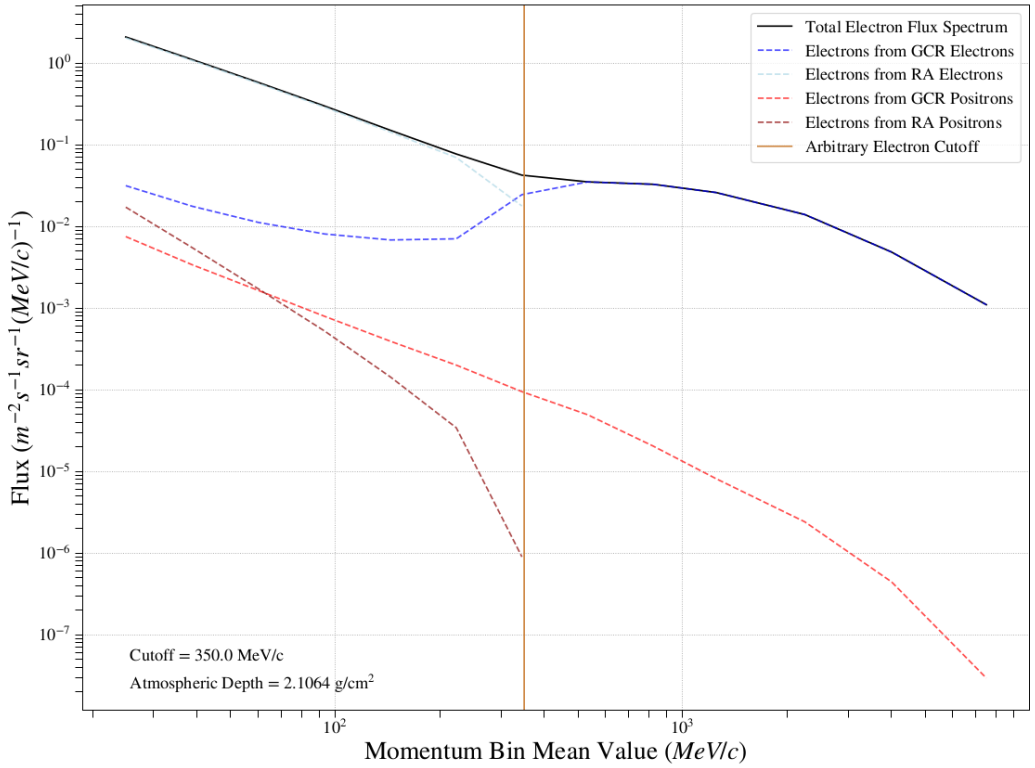

Figure 5: Estimated total flux spectrum with the spectra of the cutoff-dependent electron sources at an atmospheric depth of 2.1064 g/cm^2. An arbitrary cutoff of 350 MeV/c is applied to each source to illustrate the spectra at a higher cutoff.

spectrum is dominated by the electrons from RA electrons. Electrons from GCR electrons dominate at energies above the cutoff, as the flux from RA electrons drop off to zero. This is due to the fact that RA electrons cannot penetrate the atmosphere if their energy is less than the cutoff.

Figure 6 show the results of the fit between the expected spectrum from the five distributions and the measured spectrum from the 2018 flight. It also displays the estimated cutoff from the 2018 flight and the cutoff determined by the minimum χ^2 value. The fitted cutoff does not fall within the 2018 estimated range. There are a number of assumptions made during the process of generating the estimated spectrum that may account for the difference in cutoff. When applying the artificial cutoff to the flux sources, we assume a step function in the weighing of the flux contribution. For example, the RA flux at energies below the cutoff is defined as zero, and at energies above the cutoff the flux is at its full estimated value at that depth. In reality the distribution of weight may be more continuous instead of a distinct jump between zero and one, changing the final flux estimation.

5. Conclusion

By considering the different sources of electrons and positrons found in the atmosphere, we developed a model of the expected flux spectrum at different atmospheric depths. We compare our expected flux spectra to measurements made by AESOP-Lite during its 2018 campaign. By applying an artificial cutoff to the different sources, we can use a χ^2 minimization to determine at

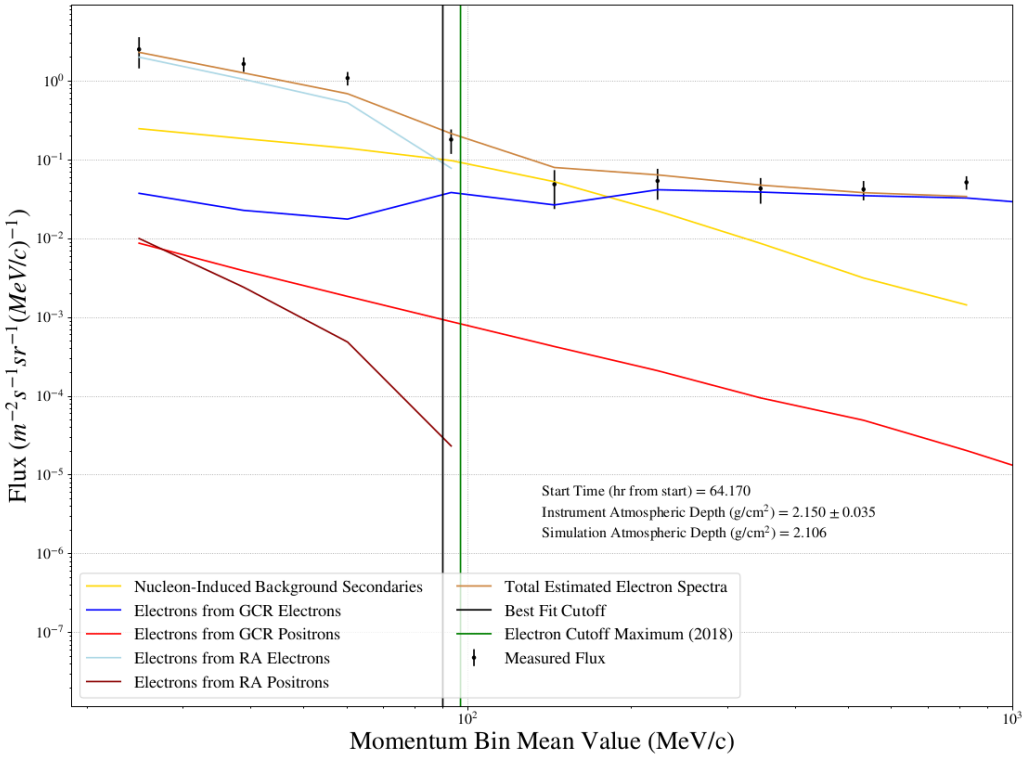

Figure 6: Estimated total electron flux spectrum fitted to the electron flux spectrum measured by AESOP-Lite in 2018 during a single 30 minute time interval. The best fit cutoff (black) and the cutoff calculated in 2018 (green) are included, as well as the five flux sources contributing to the estimated spectrum.

which cutoff our expected spectra best matches the observed spectra. Further analysis is necessary to improve upon the expected flux model. The goal of this analysis is to develop a method of determining the geomagnetic cutoff to compare with results from future cosmic ray observations.

References

[1] Jokipii, J. R., L'Heureux, J., & Meyer, P. 1967, JGR, 72, 4375

[2] Kiraly, P. et al. 1971, J. Phys. A: Gen. Phys, 4, 367

[3] Lin, Z., Bieber, J. W., & Evenson, P. 1995, JGR, 100, 23543

[4] Mechbal, S. et al. 2020, ApJ, 903, 21

[5] Simnett, G. M. & McDonald, F. B., ApJ, 1969, 157, 1435

[6] Tsyganenko, N. 1987, P&SS, 35, 1347